# Design of THz Antennas for a continuous-wave interdigitated electrode photomixer

*Document Version:*
Publisher's PDF, also known as Version of Record (includes final page, issue and volume numbers)

*Please check the document version of this publication:*

• A submitted manuscript is the version of the article upon submission and before peer-review. There can be important differences between the submitted version and the official published version of record. People interested in the research are advised to contact the author for the final version of the publication, or visit the DOI to the publisher's website.
• The final author version and the galley proof are versions of the publication after peer review.
• The final published version features the final layout of the paper including the volume, issue and page numbers.

[Link to publication](#)

# Design of THz Antennas for a Continuous-Wave Interdigitated Electrode Photomixer

M. Imran Kazim [#1], Peter Uhd Jepsen [*2], Viktor Krozer [*3]

[#]*Electromagnetics and Wireless (EMW), Department of Electrical Engineering*
*Technische Universiteit Eindhoven (TU/e), P.O. Box 513, 5600 MB Eindhoven, The Netherlands*
[1]`m.i.kazim@tue.nl`

[*]*Department of Photonics Engineering–Department of Electrical Engineering*
*Technical University of Denmark (DTU), DK-2800 Kgs. Lyngby, Denmark*
[2]`puje@fotonik.dtu.dk`
[3]`vk@elektro.dtu.dk`

*Abstract*— **The design of a dual-slot antenna integrated with an interdigitated electrode (IDE) LT GaAs photomixer together with choke filters and a dielectric lens, optimized for high output power at an operating frequency of 1 THz is proposed. An equivalent-circuit model for determination of coplanar waveguide (CPW) IDE capacitance is suggested, in order to tune it out using a dual-slot antenna. The initial design based on a Smith chart approach has been validated by carrying out exhaustive simulations in CST MicroWave Studio software. The radiation efficiency, incase of a dual-slot antenna integrated with a lumped capacitor element is found to be 81% with a directivity value of 11.47 dBi. The effect of choke filters on different antenna radiation parameters is also investigated. A 3-fan CPW radial stub gives a radiation efficiency of 62% with a directivity of 10.5 dBi and has a potential of providing better performance.**

## I. INTRODUCTION

Photomixers are finding applications as continuous-wave (CW) THz radiation source for high-resolution spectroscopy, imaging systems and as a local oscillator on future space-borne heterodyne receivers etc. [1], [2], [3], [4]. The system configuration of a typical photomixer setup is shown in Fig. 1. The design of a CW photonic THz antenna is not possible without understanding of the photomixer operation and devices. The state-of-the-art LT GaAs interdigitated electrode photomixer has been selected for its relative ease of fabrication, and a potential of giving useful output powers for most of the applications at THz frequencies. A lot of research has been carried out to optimize LT GaAs design, but most approaches are based on an improved heat sinking to allow for a higher optical input power. The low output power of a photomixer at high frequencies is a result of -6 dB/octave roll-off arising from the lifetime of the carriers and a reduction in load impedance due to the $R_{ant}C_{elec}$ time constant (another -6 dB/octave roll-off). The 'shorting out' of the load impedance by photomixer capacitance makes it increasingly difficult to couple power into an external circuit. The increased antenna resistance and tuning out the electrode capacitance play a pivotal role in the design of an efficient high output power THz emitter. Dipole and slot antennas, used as single and dual elements, have significant power advantages over log-spiral designs, when large bandwidths are not necessary [5].

However, the inductive tuning used by these antenna elements to tune out the electrode capacitance at the desired frequency requires the determination of interdigitated electrode capacitance. Antennas on planar dielectric substrates suffer from power loss to substrate modes which can be eliminated using a semi-infinite dielectric substrate [6].

Section II presents an approach for capacitance determination of CPW interdigitated electrode geometry. The detailed design and simulation of a dual-slot antenna at 1 THz operating frequency is explained in Section III. Section IV illustrates different choke filter schemes and the simulation results of a THz emitter. Finally, the conclusion is made.
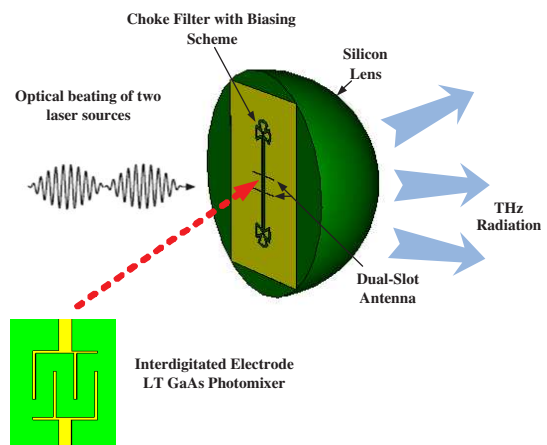


Fig. 1. Photomixer operation

## II. CPW IDE CAPACITANCE DETERMINATION

The interdigitated electrode geometry possesses a capacitance that presents a key design challenge for providing high output power and strongly affects the behavior of the photomixer-integrated-antenna at THz frequencies. The prediction of quasi-static interdigitated electrode capacitance using a conformal mapping technique suffers from limitations of ignoring the metallization thickness, end-capacitance and high frequency effects [7]. In this section, an approach for

| # | Interdigitated Electrode Geometry | | | | | Approaches | | | |
|---|---|---|---|---|---|---|---|---|---|
| | $N_f$ | $W_f$ ($\mu$m) | $W_g$ ($\mu$m) | $L_f$ ($\mu$m) | $t$ ($\mu$m) | Quasi-Static Approx. Cap.(fF) | CST MicroWave Studio | | |
| | | | | | | | Cap.Range (0.2 - 2 THz) | Constant Cap. | |
| | | | | | | | | Range(THz) | Val.(fF) |
| 1 | 4 | 0.2 | 1.4 | 3.6 | 0.5 | 0.359 | 0.6351 - 0.9314 | 0.9980 - 1.0620 | 0.71 |
| 2 | 4 | 0.2 | 1.4 | 3.6 | 0.005 | | 0.4974 - 0.7177 | 0.9320 - 1.0140 | 0.55 |
| 3 | 6 | 0.2 | 0.85 | 4.6 | 0.5 | 0.8862 | 1.181 - 2.346 | 0.9980 - 1.0320 | 1.35 |
| 4 | 5 | 0.2 | 1 | 4 | 0.5 | 0.58786 | 0.871 - 1.328 | 0.9640 - 1.010 | 0.97 |
| 5 | 4 | 0.24 | 1.76 | 6.24 | 0.5 | 0.61216 | 0.754 - 1.702 | 0.9740 - 1.0040 | 0.90 |
| 6 | 4 | 0.2 | 1.4 | 3.6 | 0.1 | 0.3585 | 0.440 - 0.695 | 0.9340 - 1.0040 | 0.50 |
| 7 | 4 | 0.2 | 1.76 | 6.24 | 0.1 | 0.577 | 0.753 - 2.870 | 0.9820 - 1.0020 | 0.97 |
| 8 | 6 | 0.2 | 0.976 | 7.024 | 0.1 | 1.29 | 1.215 - 4.008 | 0.990 - 1.0010 | 1.7105 |
| 9 | 8 | 0.2 | 0.91428 | 7.0857 | 0.1 | 1.8450 | 1.54 - 3.5 (1.3 THz) | 0.9780 - 1.0160 | 2.3 |
| 10 | 4 | 0.2 | 2.933 | 7.2 | 0.1 | | 0.92 - 2.24 (1.5 THz) | 0.90 - 1.0400 | 1.22 |
| Inclusion of 1 $\mu m$ thick Electrode Frame | | | | | | | | | |
| 11 | 4 | 0.2 | 1.4 | 3.6 | 0.5 | 0.359 | 0.637 - 1.334 | 0.9960 - 1.0300 | 0.76 |
| Fish-Bone Interdigitated Electrode Structure | | | | | | | | | |
| 12 | 4 | 0.2 | 2.933 | 7.2 | 0.1 | | 0.63 - 1.36 (1.5 THz) | 0.98 - 1.0040 | 0.81 |
| Gap Capacitance of 25 $\mu m^2$ Active Area | | | | | | | | | |
| 13 | - | | | | | | 0.1428 - 0.2086 | 0.9980 - 1.1540 | 0.18 |

capacitance determination of IDE geometry is presented. The premise of the proposed approach is provided by a standard $\pi$-equivalent circuit for a two-port CPW series gap. CST model of CPW IDE geometry is delineated in Fig. 2. $T_1$ and $T_2$ represent the reference planes of a two-port interdigitated electrode geometry.

The proposed circuit model of CPW interdigitated electrode geometry is also shown in Fig. 2, for which a pure capacitive $\pi$-network is considered. Interdigitated electrode capacitance $C_{elec}$ depends on the size and number of electrode fingers geometry. The parasitic capacitances $C_{p1}$ and $C_{p2}$ of CPW interdigitated electrode geometry are independent of the size and number of electrode fingers and they can be minimized by varying the location of ground planes [8].

As interdigitated electrode capacitance $C_{elec}$ is of prime interest for tuning purposes, it can be determined from the Y-parameters as $C_{elec} = \frac{-Imag\{Y_{12}\}}{2\pi f}$. The use of this approach makes the calculation of interdigitated electrode capacitance $C_{elec}$ independent of any structural geometry between the two reference planes $T_1$ and $T_2$. Moreover, additional capacitance due to interdigitated electrode frames can also be incorporated by recalculating the S-parameters and modelling them into parasitic capacitances. A number of CPW IDE geometries have been simulated in CST MicroWave Studio by varying number of fingers $N_f$, finger-width $W_f$, gap-width $W_g$, finger-length $L_f$ and metallization thickness $t$. The comparison of capacitance is provided in Table I.

## III. DESIGN OF A DUAL-SLOT ANTENNA

The systematic design procedure of a dual-slot antenna is presented in this section. The dual-slot antenna placed on a silicon substrate lens for avoidance of the excitation of substrate modes, is designed. The relative permittivity of silicon has been used in the calculations, since the printing of
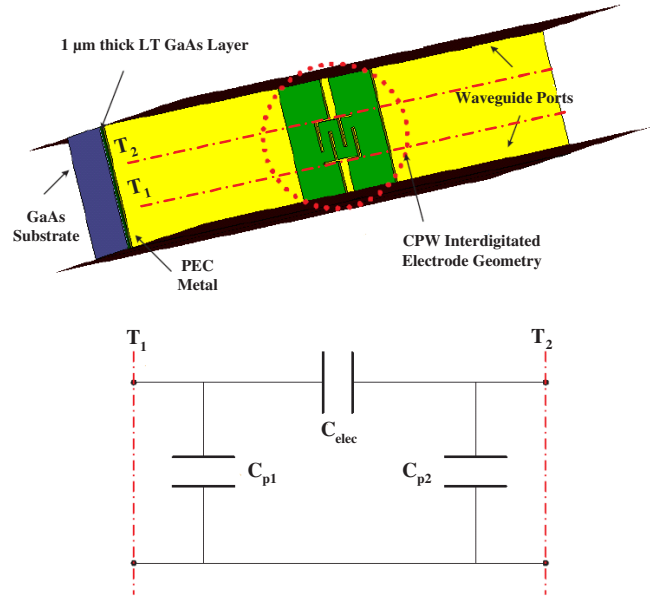


Fig. 2. CST model of an IDE photomixer and proposed pure capacitive $\pi$-network

antenna structure is done on GaAs substrate, which has a much smaller thickness as compared to semi-infinite silicon lens. Reference [9] shows an equivalent-circuit model of a dual-slot antenna, integrated with a photomixer and a choke filter. A coplanar waveguide is used as the connecting transmission line, and bias is applied across the electrodes. The slots are connected in series, making the input impedance twice that of a single-slot arm. The Smith chart has been used as a starting point for the design of a dual-slot antenna, followed by exhaustive simulations in CST MicroWave Studio software. The metallization thickness and mutual coupling have also

been incorporated in the design, which were absent in the previous design approaches [9]. Table II tabulates the initial design values of a dual-slot antenna integrated with an IDE photomixer.

## A. Smith Chart Design Procedure

An admittance Smith chart has been used to calculate the length of CPW, connecting the IDE photomixer and a slot arm, for tuning out the electrode capacitance. Figure 3 delineates the following steps, used for determination of CPW connecting-line length $L_{con}$.

- Normalization of single-slot antenna admittance with respect to $Z_{cpw}$ (shown as point A in the Smith chart).
- Determination of $C_{elec}$ using the proposed approach in Section II (shown as point B in the Smith chart).
- Normalization of electrode susceptance with respect to $Z_{cpw}$, i.e., $b_{elect} = j2\pi f C_{elect} Z_{cpw}$ which leads to $b_{goal} = -j2 b_{elect}$ (shown as point C in the Smith chart).
- Drawing of a constant refection coefficient circle, connecting $y_{slot}$ and $b_{goal}$, yielding the transformed admittance $y_{trans}$ and the CPW connecting-line length (shown as line D in the Smith Chart).
- Determination of radiation resistance $R_{rad}$ (assuming radiation efficiency $e_{rad} = 1$), i.e., $R_{rad} = 1/(\frac{g_{trans}}{2Z_{cpw}})$.



Fig. 3. Smith chart design procedure

TABLE II
CALCULATED VALUES FOR THE DUAL-SLOT ANTENNA DESIGN

| Parameter | Value | Calculation |
|---|---|---|
| operating frequency $f$ | 1 THz | |
| metallization thickness $t$ | 0.1 $\mu m$ | |
| relative permittivity of Si $\epsilon_r$ | 11.9 | |
| free-space wavelength $\lambda_o$ | 300 $\mu m$ | $\lambda_o = c/f$ |
| mean wavelength $\lambda_m$ | 120 $\mu m$ | $\lambda_m = \frac{\lambda_o}{\sqrt{\epsilon_{eff}}}$ |
| coplanar waveguide (CPW) | | |
| *centre conductor strip $S$* | 1 $\mu m$ | |
| *gap-width $W$* | 6 $\mu m$ | |
| *characteristic impedance $Z_{cpw}$* | 89 $\Omega$ | [10] |
| *Efft. dielectric constant $\epsilon_{eff}$* | 6.25 | [10] |
| IDE capacitance $C_{elec}$ | 0.60 fF | Section II |
| length of a slot antenna $L_{slot}$ | 103 $\mu m$ | [11] |
| width of a slot antenna $W_{slot}$ | 1 $\mu m$ | [11] |
| input impedance | 15 $\Omega$ | [11], [12] |
| *after mutual coupling $Z_{in}$* | 16.66 $\Omega$ | |
| CPW connecting-line $L_{con}$ | 17.76 $\mu m$ | Smith chart |
| radiation resistance $R_{rad}$ | 570 $\Omega$ | Smith chart |

## B. CST MicroWave Studio Simulations

The exhaustive design simulations of a dual-slot antenna have been carried out in CST MWS using both PEC and lossy gold metal. The detailed design procedure and problems encountered during simulations with remedial solutions are mentioned in [13]. A parameterized model of a dual-slot antenna on a silicon substrate lens has been constructed in CST MWS software, as shown in Fig. 4. Transient solver with a frequency sweep from 0 to 2 THz has been used for simulation purposes. In order to enable a transient calculation, a discrete port is defined as the excitation source, feeding the
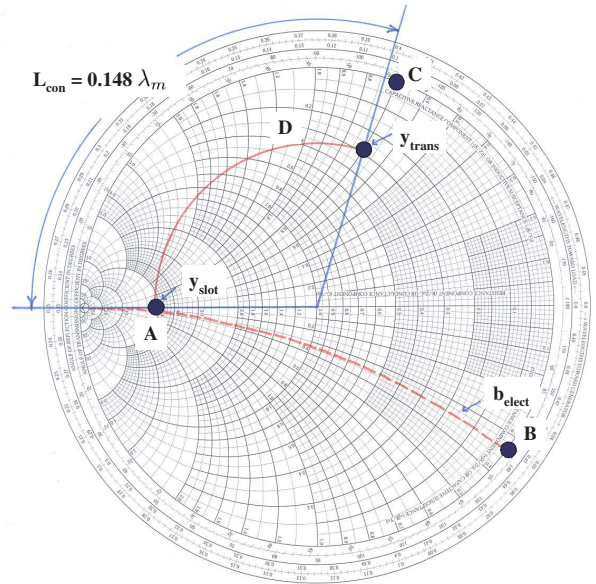
dual slot antenna. The interdigitated electrode capacitance has been modelled as a lumped capacitor element.
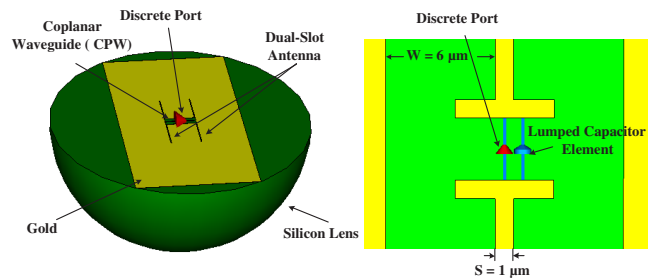


Fig. 4. CST model of a dual-slot antenna on a silicon substrate lens with a lumped capacitor

The initial design values are taken from Table II. The length of CPW connecting-line has been optimized for increased directivity and radiation efficiency of a dual-slot antenna, using CST MicroWave Studio software. The far-field patterns are plotted for a structure consisting of a dual-slot antenna on a substrate lens having lossy gold metallization thickness of 0.1 $\mu m$, with a lumped capacitor element of 0.60 fF, as shown in Fig. 5. The far-field pattern for 1.01 THz shows a maximum radiation for $\theta$ (theta) $= -180^o$ (into the silicon substrate lens). The radiation efficiency is found to be 81% with a directivity value of 11.47 dBi. The radiation efficiency is 100%, incase of a PEC metal. The E-plane and H-plane patterns are symmetrical with low side-lobe values, i.e. SLL = -13.1 dB.

## IV. THz EMITTER - SIMULATION RESULTS

The use of a proper biasing scheme plays a pivotal role in determining the overall efficiency of a THz emitter. THz
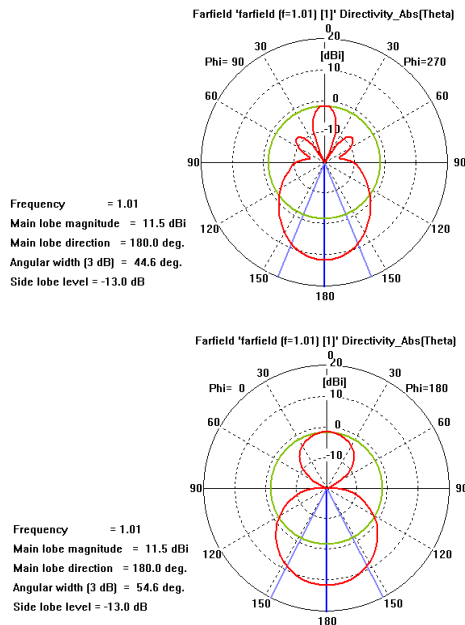
Fig. 5. E-plane and H-plane patterns of a dual-slot antenna on a silicon substrate lens with a lumped capacitor of 0.60 fF

leakage down the bias line can be minimized using different choke filters. This section gives an overview of different THz choke filter schemes along with the effect of each approach on the radiation pattern of a THz emitter comprising a dual-slot antenna, interdigitated electrode capacitor and the choke filter.

### A. Quarter-Wave Choke Filter

A quarter-wave choke is a stepped-impedance filter, consisting of high- and low-impedance sections. The length of each high- and low-impedance section corresponds to $\lambda_m/4$. The choke filter is employed to present a 'short circuit' for the THz current at the interface with the radiating slot.

The radiation efficiency observed using a quarter-choke filter is 41%, owing to high radiation losses, thereby implying the inherent disadvantage of using this approach. The E-plane and H-plane patterns preserve symmetry due to the fully symmetrical structure. The low side-lobe levels of -15.1 dB and -13.5 dB for E-plane and H-plane, respectively with a directivity of 10.9 dBi are observed.

### B. Single CPW Radial Stub

The principle of a single CPW radial stub can be best understood from Fig. 6. THz signal can be prevented from escaping through the DC network by the use of a $\lambda_m/4$ or $3\lambda_m/4$ transmission line, in conjunction with a $\lambda_m/4$ radial stub. THz short circuit is created at the point, where $\lambda_m/4$ radial stub is attached to the transmission line. THz signal experiences very low impedance (virtual ground) at this point. The connection of this known low impedance to a $\lambda_m/4$ or $3\lambda_m/4$ transmission line results in the generation of a THz signal high impedance (open circuit) point, at the opposite end of the transmission line, as delineated in Fig. 6.

A much better radiation efficiency of 78%, in comparison with a quarter-choke filter, has been observed. However, an asymmetrical pattern of the H-plane has been noticed, primarily due to the asymmetrical nature of the structure. The H-plane pattern is tilted at an angle of $165^o$.

### C. 3-Fan CPW Radial Stub

A 3-fan CPW radial stub is shown in Fig. 7. The central stub of a 3-fan CPW radial stub scheme acts as a DC bias pad.
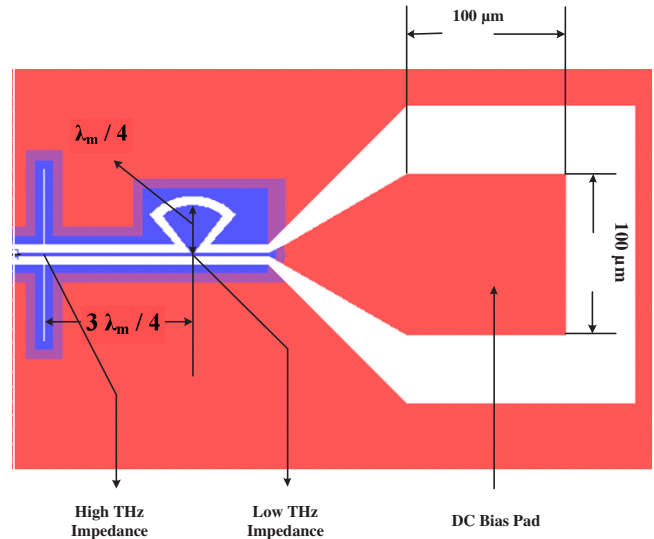
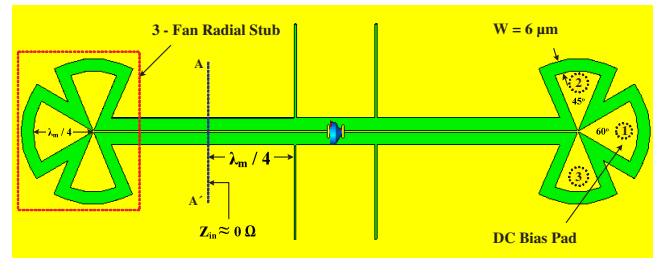Fig. 6. Principle of a single CPW radial stub

Fig. 7. 3-fan CPW radial stub

A radiation efficiency of 62% with a directivity of 10.5 dBi has been observed. The relatively decreased radiation efficiency can be ascribed to the complex structural geometry of a 3-fan CPW radial stub. The patterns of E-plane and H-plane are symmetrical due to symmetrical nature of the structure. The SLL are noted to be -6.3 dB and -8.3 dB for the E-plane and H-plane pattern, respectively. The 3-fan CPW radial stub has been simulated by keeping the central radial stub angle of $60^o$. The angles of stubs 2 & 3 are varied at $45^o$ and $30^o$ for two different simulations. The structure of 3-fan CPW radial stub is hard to parameterize, due to difficulty of definition of a parametric polygon in CST MWS. However, a parameterized CPW transmission line attached with the radial stub and an excited waveguide port has been used to determine

1643

**Farfield 'farfield [f=0.97] [1]' Directivity_Abs[Theta]**

Frequency = 0.97
Main lobe magnitude = 10.5 dBi
Main lobe direction = 180.0 deg.
Angular width (3 dB) = 26.5 deg.
Side lobe level = -6.3 dB

**Farfield 'farfield [f=0.97] [1]' Directivity_Abs[Theta]**

Frequency = 0.97
Main lobe magnitude = 10.5 dBi
Main lobe direction = 180.0 deg.
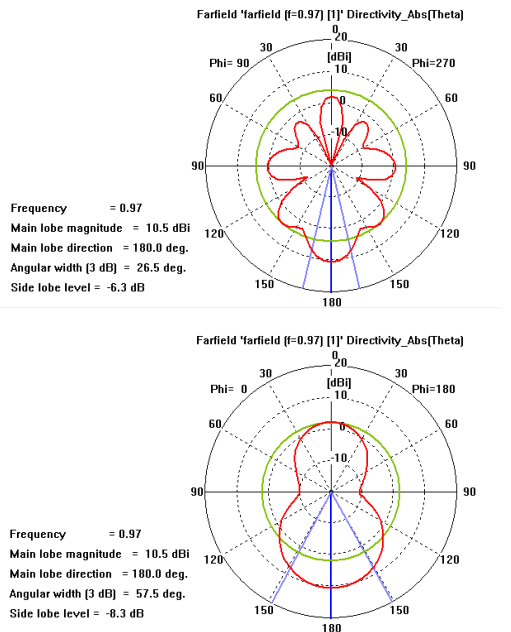Angular width (3 dB) = 57.5 deg.
Side lobe level = -8.3 dB

Fig. 8. E-plane and H-plane patterns of a dual-slot antenna on a silicon substrate lens with a lumped capacitor of 0.9745 fF and a 3-fan CPW radial stub

the input impedance of a 3-fan CPW radial stub. The input impedance, incase of a lossy gold metal, as seen from the reference plane A-A′(shown in Fig. 7) is determined to be 10 $\Omega$ with a small imaginary part of impedance. Ideally, the input impedance should be 0 $\Omega$. However, the input impedance of 2-3 $\Omega$ can be achieved by the variation of angles and radius of the three radial stubs.

## V. CONCLUSIONS

The detailed design presented in this thesis can be scaled up for frequencies greater than 1 THz. An approach for determination of CPW interdigitated electrode capacitance is presented. The design of a resonant dual-slot antenna is desirable because of its symmetrical patterns, increased radiation resistance and provision of tuning out the interdigitated electrode capacitance, which results in increased THz output power at a desired operating frequency. The 3-fan CPW radial stub has a potential of providing better performance but its optimization in terms of input impedance close to 0 $\Omega$, still needs to be investigated. The use of wider CPW connecting-line between slot antenna and choke filter can remove discrepancy in H-plane pattern by physically shorting the current at the interface of radiation slot. The incorporation of air bridges can ensure the same ground plane level for proper mode propagation. It is expected that an improved heat sinking together with a resonant dual-slot antenna and a 3-fan CPW radial stub scheme can significantly increase the THz output power of LT GaAs interdigitated electrode photomixer at a desired frequency. The study in this paper is based on 3-D EM simulation. The fabrication of the emitter followed by measurements will enable determination of THz output power

and realizable bandwidth around the centre frequency of 1 THz.

## REFERENCES

[1] V. Krozer, B. Leone, H. Roskos, G. Loata, F. Renner, S. Eckardt, S. Malzer, T. O. Klaassen, A. Adam, P. Lugli, A. D. Carlo, M. Manenti, G. Scamarcio, M. S. Vitiello, and M. Feiginov, "Optical Far-IR Wave Generation - State-of-the-Art and Advanced Device Structures," *Proceedings of SPIE*, vol. 5466, 2004.

[2] "Optical far-infrared wave generation," Rutherford Appleton Laboratory, Tech. Rep., 2002.

[3] E. R. Brown, "THz Generation by Photomixing in Ultrafast Photoconductors," *International Journal of High Speed Electronics and Systems*, vol. 13, no. 2, pp. 497–545, 2003.

[4] I. S. Gregory, C. Baker, W. R. Tribe, I. V. Bradley, M. J. Evans, E. H. Linfield, A. G. Davies, and M. Missous, "Optimization of Photomixers and Antennas for Continuous-Wave Terahertz Emission," *IEEE Journal of Quantum Electronics*, vol. 41, no. 5, May 2005.

[5] D. Mittleman, *Sensing with Terahertz Radiation*. Springer, 2005.

[6] G. M. Rebeiz, "Millimeter-Wave and Terhertz Integrated Circuit Antennas," *IEEE Proceedings*, vol. 80, no. 11, November 1992.

[7] Y. C. Lim and R. A. Moore, "Properties of alternately charged coplanar parallel strip by conformal mapping," *IEEE Transactions on Electronic Devices*, vol. 15, no. 173, 1968.

[8] M. Naghed and I. Wolff, "Equivalent Capacitances of Coplanar Waveguide Discontinuities and Interdigitated Capacitors Using a Three-Dimensional Finite Difference Method," *IEEE Transactions on Microwave Theory and Techniques*, vol. 38, no. 12, December 1990.

[9] S. M. Duffy, S. Verghese, K. A. McIntosh, A. Jackson, A. C. Gossard, and S. Matsuura, "Accurate Modeling of Dual Dipole and Slot Elements Used with Photomixers for Coherent Terhertz Output Power," *IEEE Transactions on Microwave Theory and Techniques*, vol. 49, no. 6, June 2001.

[10] R. Garg, P. Bhartia, I. Bahl, and A. Ittipiboon, *Microstrip Antenna Design Handbook*. Artech House, 2001.

[11] G. V. Eleftheriades and G. M. Rebeiz, "Self and Mutual Admittance of Slot Antennas on a Dielectric Half-Space," *International Journal of Infrared and Millimeter Waves*, vol. 14, no. 10, July 1993.

[12] R. E. Collin, *Antennas and Radiowave Propagation*. McGraw-Hill, Inc., 1985.

[13] M. I. Kazim, "Design of continuous-wave photonic terahertz antennas," MS thesis, Denmark Technical University, Kgs. Lyngby, Denmark, 2006.